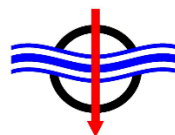
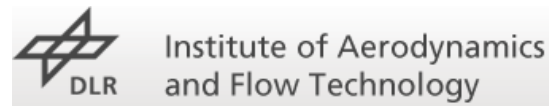


Executive Summary: Testing of MLI

Document No.:	D4DBB-OHB-ES-002
Issue:	01
Date:	01.04.2022
CI No.:	
AD No.:	



Name	Responsibility	Signature	Date
Prepared by:			
D4DBB Team			
Bradley Lockett	MMPP Engineer		
Checked by:			
Britta Ganzer	Project Manager		
Approved by:			
Britta Ganzer	Project Manager		

Distribution List

Name	No. of Copies	Company/Organization
A. Caiazzo	1	ESA

Document Change Record

Issue	Date	Change Description/Reason (Ref.)	Page/Chapter Affected
draft	01.04.2022	First Issue	all

Table of Contents

1	INTRODUCTION	7
1.1	Overview D4D Breadboarding Activity.....	7
1.2	CCN Activity - Testing of MLI	8
2	ABBREVIATIONS & NOMENCLATURE.....	9
3	STUDY SCHEDULE AND LOGIC	10
4	MLI TECHNOLOGIES TESTED	11
4.1	Standoffs.....	11
4.2	Velcro.....	13
5	SAMPLE PREPARATION	14
6	ATOX TESTING	16
6.1	ATOX Test Samples.....	16
6.2	Testing Results – ATOX Exposure	18
7	STATIC RE-ENTRY TESTING	24
7.1	Test Conditions Derivation	25
7.2	Static Re-entry Substrate Design	26
7.3	Static Re-entry Testing.....	27
8	LESSONS LEARNED.....	36
9	CONCLUSION.....	37

List of Tables

Table 2-1: Abbreviations & Nomenclature	9
Table 3-1: Work Breakdown and Schedule.....	10
Table 4-1: Intended testing of ATOX specimen	11
Table 5-1: Specimen Material Configuration.....	14
Table 6-1: as-manufactured ATOX sample information (courtesy of RUAG-A).....	17
Table 6-2: fluence variation experienced on each sample	18
Table 6-3: pre and post ATOX testing thermo-optical properties	20
Table 6-4: sample mass loss and corresponding atomic oxygen erosion yield experienced.....	20
Table 6-5: relative erosion yield data	21
Table 6-6: SEM imaging before and after ATOX exposure	21
Table 7-1: heat flux trajectory profile (HF TRAJ).....	25
Table 7-2: Sample specifications for re-entry demisability testing.....	29

List of Figures

Figure 4-1: Schematic view of MLI attached to substrate using standoffs	11
Figure 4-2: Generic dimensions of RUAG Standoffs, dependent of application and purpose	12
Figure 4-3: MLI layup configurations and their respective schematic diagrams	12
Figure 4-4: picture of ATOX MLI sample attached with Velcro	13
Figure 5-1: Characterisation specimen: 80 mm x 80 mm x 20 mm; Through Spool insert.....	15
Figure 5-2: Manufactured CFRP sample with through spool insert	15
Figure 5-3 - Phenomenology specimen setup: 160 mm x 160 mm x 20 mm per panel; Cleat Joint via Through Spool and Surface Inserts (right: example of assembled CFRP panel setup)	15
Figure 6-1: schematic of the ESTEC LEOX test facility.....	16
Figure 6-2: All samples as prepared from Invent	17
Figure 6-3: pre-testing image of ATOX samples mounted to testing fixture	18
Figure 6-4: expectation of fluence applied across test samples	19
Figure 6-5: post-testing image of ATOX samples mounted to testing fixture	19
Figure 6-6: ITO-SiO _x MLI sample utilising standoff mounting technologies post-ATOX exposure.....	20
Figure 6-7: SEM measurement locations for ACKTAR black MLI sample	22

Figure 6-8: visual inspection of Velcro connection patches post-ATOX exposure.....23

Figure 6-9: untested ITO-SiOx MLI blanket23

Figure 6-10: ATOX MLI samples post-testing with noticeable appearance change highlighted.....23

Figure 6-11: bright stripes observed on the outer layer of ITO-SiOx MLI23

Figure 7-1: mechanical loading in chamber24

Figure 7-2: the 80 x 80mm sample holder as designed26

Figure 7-3: picture with modified 80 x 80mm sample holder26

Figure 7-4: images showing use of sample mounting solutions (samples from previous D4D-BB testing).....27

Figure 7-5: corner sample (with standoffs) post-static re-entry testing.....30

Figure 7-6: Calibration Blocks (CCN, left, and BB test campaign 2, right).....30

Figure 7-7: Baseline data, left, vs Nominal MLI, right)31

Figure 7-8: Nominal MLI (Standoffs, left, vs Velcro, right).....31

Figure 7-9: Nominal MLI vs Kapton Black (right), both utilising standoffs.....32

Figure 7-10: Nominal MLI vs Kapton Black (right) with Velcro32

Figure 7-11: Baseline vs ACKTAR Black (right).....32

Figure 7-12: removal of bolt and threaded sleeve from the demisable insert body.....33

Figure 7-13: temperature measurements of demisable insert sample (Test ID 9).....33

Figure 7-14: post-test damage of corner sample34

Figure 7-15: temperature data from corner sample test.....34

Figure 7-16: comparison of bare CFRP stripe and ATOX sample (Test ID 4) stripe35

1 INTRODUCTION

1.1 Overview D4D Breadboarding Activity

Rising space debris populations have been recognized as a significant issue for the space community. A breadth of mitigation methods have been assessed such as moving satellites to safe long-term orbits at the end of their active life or disposing of them via re-entry either actively or within reasonable timeframes after life. The second is preferred for spacecraft in Low Earth Orbits (LEO) as they do not require additional systems or significant propellant allocations. The downside is that they pose a risk to the human population when they re-enter.

In order to maintain levels of space debris which are acceptable, requirements are imposed upon spacecraft which require that they are reentered within 25 years or placed into safe orbits if the spacecraft are within specific protected regions. Further to this, a requirement that the casualty risk must be below 10^{-4} is specified. This is avoided for controlled de-orbits where the safety constraints are met by ensuring that the spacecraft (in its fragmented state) impacts safe areas such as the ocean. Controlled re-entry comes with the additional burdens of mass and cost and must be performed whilst the spacecraft is still operational. Uncontrolled re-entry naturally has benefits in terms of being passive and not requiring additional systems, propellant, or to be operational when re-entry occurs. The ability to maintain operability as long as possible is naturally a significant advantage for many space missions.

As was considered and assessed in previous studies, the opening of the outer satellite structure during or prior to re-entry helps to reduce the casualty risk on ground. In order to effectively investigate techniques and technologies to open and/or release external elements, an understanding of the mechanisms at play on these elements during re-entry is needed. In order to achieve this, a review of current relevant joining technologies was carried out to select a number of these for testing. An array of morphological tests was then planned and carried out to characterize these technologies using re-entry simulation chambers.

Following this, development of feasible design concepts to achieve structure break-up or opening at an altitude above the natural break-up altitude was carried out. A selection of these were then developed into breadboard models and tested in order to assess feasibility and effectiveness.

Whilst previous studies focused on a system level overview and the potential impacts of different technologies and techniques for D4D, this study and testing focuses on obtaining results to inform the future selection and implementation of passive technologies, active technologies, and demisable joining technologies.

The objective of the activity is to demonstrate feasibility of design concepts to achieve spacecraft break-up or structure opening at a higher altitude than occurs with current designs. The work performed has suggested that the break-up altitudes of sandwich-panel based spacecraft structures are likely to be higher than the nominal 78km value which is used in many current risk assessments, and could be further promoted by use of the breadboarded design concepts.

1.2 CCN Activity - Testing of MLI

Although the outcome of the main activity is positive, a risk has been identified. The multi-layer insulation (MLI) which is expected to be present on most spacecraft is generally assumed to have been removed due to the interaction with atomic oxygen in the atmosphere during the mission lifetime and orbital decay phase, or if not, to be removed by the low forces in the very initial stages of re-entry. Given the high altitudes identified for the potential structural break-ups, the presence of MLI can have a significant impact in delaying the heat soak to the structure and thus the fragmentation of the spacecraft. Therefore, in order to verify the performance of the early structure break-up breadboards, an assessment of the MLI behaviour is required. This assessment is the objective of CCN activity of the D4D Breadboarding project.

In order to capture this behaviour, two steps were proposed. The first was to obtain an understanding of the state of the MLI material after the mission and orbital decay timescale. This was done using the ESTEC ATOX facility which can provide a fluence of atomic oxygen to a set of material samples. In this case, the MLI is quite resistant to the atomic oxygen, which is not always the case, but the connection to the spacecraft is significantly damaged. Failure of the connection allowing the MLI to be released is an ideal scenario for early spacecraft break-up.

As well as the impact on MLI materials, there is also the possibility to assess the impact of atomic oxygen on spacecraft surfaces in the case that the MLI is considered to have been removed. The impact on metallic surfaces (aluminium panels) is expected to be limited to the formation of an oxide layer, which is also seen in wind tunnel testing. The impact on composite surfaces (CFRP panel facesheets) is significantly more interesting. Here, a reaction of the carbon fibres is possible which can reduce the integrity of the panel resulting in a faster break-up. As the destructive processes of CFRP materials are not well understood, this provides an excellent opportunity to gain some useful data on the fibre behaviour.

The fluence required for the atomic oxygen test will be at the upper end of the facility capability due to the long decay time (up to 25 years) and the higher atmospheric densities at lower altitudes which are encountered in the final days before re-entry.

The second part of the activity is to assess the impact of MLI presence on the structural break-up. This will be done by extending the test campaign at AAC to include samples with MLI attached. In order to obtain a sensitivity, samples with standard inserts will be tested as well as breadboard demisable joints. Further, tests are run with intact MLI material, and degraded MLI material in order to understand the differences which would be observed, based on the understanding from the atomic oxygen testing.

Using the data from the two test campaigns, the potential impact of the MLI on the spacecraft fragmentation was quantified. This will determine the need for assessment of MLI types, or MLI connection types, which are required to be used in order to allow the full potential of early break-up demisable joint designs to be realised.

2 ABBREVIATIONS & NOMENCLATURE

For all terms, definitions and conventions used, if available.

Table 2-1: Abbreviations & Nomenclature

Abbreviation	Meaning
AD	Applicable Document
Af	austenite finish temperature
AIT	assembly, integration and test
Al	Aluminium
As	austenite start temperature
CCU	Command and Control Unit
CFRP	Carbon Fiber Reinforced Plastic
Config.	Configuration
CTE	Coefficient of Thermal Expansion
D4D	Design for Demise
D4DBB	Design for Demise Breadboarding
ECSS	European Cooperation for Space Standardization
ESA	European Space Agency
ISO	International Organization for Standardization
LEO	Low Earth Orbit
OHB	OHB System AG
RD	Reference Document
S/C	Space Craft
SCARAB	Spacecraft Atmospheric Re-entry and Aerothermal Break-up
SoW	Statement of Work
TN	Technical Note
TRL	Technology Readiness Level

3 STUDY SCHEDULE AND LOGIC

The CCN activity was carried out according to the work schedule and tasks presented in Table 3-1. The activity was performed in two phases. First the Atox Chamber Tests were performed and in the second phase the Static Re-entry Tests were performed.

Table 3-1: Work Breakdown and Schedule

Org	Tasks	Start	End
OHB	Project Office	KO	FP
	Atox Tests		
OHB	Atox Test Preparation and Procedure	KO	PM1
BRL	Atox Test Conditions and Test Assessment	KO	PM1
INVENT	Provision of Panel Test Samples (Atox)	KO	PM1
OHB	Provision of MLI Test Samples (Atox)	KO	PM1
BRL	ATOX Tests	KO	PM1
	Static tests		
OHB	Demise Test Preparation and Procedure	PM1	FP
BRL	Reentry Test Conditions and Test Assessment	PM1	FP
INVENT	Provision of Panel Test Samples (Reentry)	PM1	FP
OHB	Provision of MLI Test Samples (Reentry)	PM1	FP
OHB	Reentry Tests	PM1	FP

4 MLI TECHNOLOGIES TESTED

There were 3 different configurations of MLI tested in both the ATOX and the re-entry campaigns, which can be seen in Table 4-1, below. These configurations are typical for a LEO mission and were provided by RUAG Austria.

Table 4-1: Intended testing of ATOX specimen

Config. Number	Test Type	MLI Configuration	Attachment Method	Size [mm x mm]
1	Control	No MLI	-	26 x 114
2	Black Kapton XC/VDA	Black Kapton outer MLI layer	Velcro	26 x 114
3	ACKTAR Black	Black paint applied to outer MLI layer	Velcro	26 x 114
4	“Nominal” MLI	ITO-SiOx outer MLI layer coating	Velcro	26 x 114
5	“Nominal” MLI	ITO-SiOx outer MLI layer coating	Stand-offs	26 x 114

4.1 Standoffs

MLI secured by a standoff and clip washer is the first tested method of fixing MLI to a satellite.

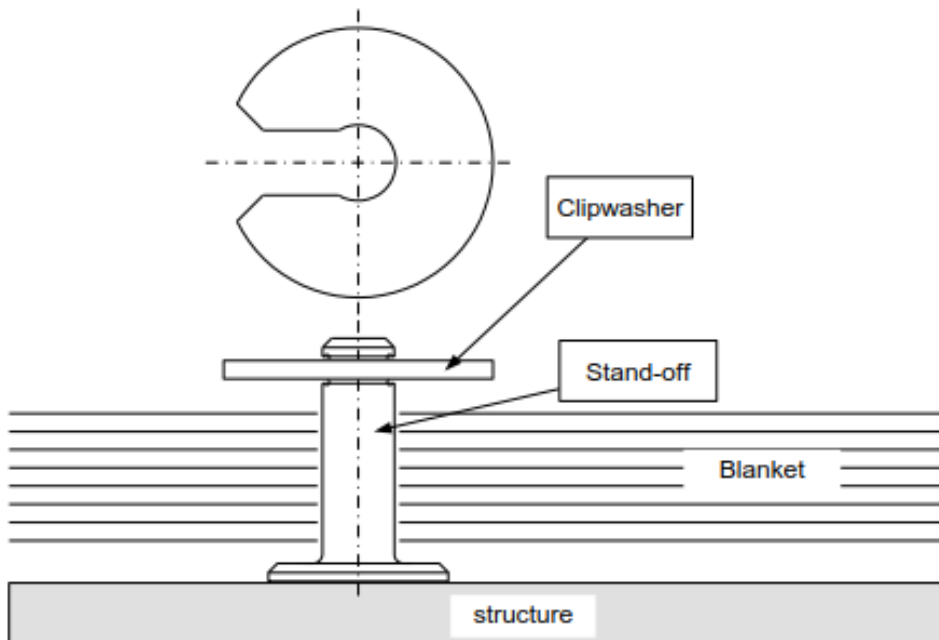


Figure 4-1: Schematic view of MLI attached to substrate using standoffs

The dimensions of the RUAG standoffs is shown in Figure 4-2.

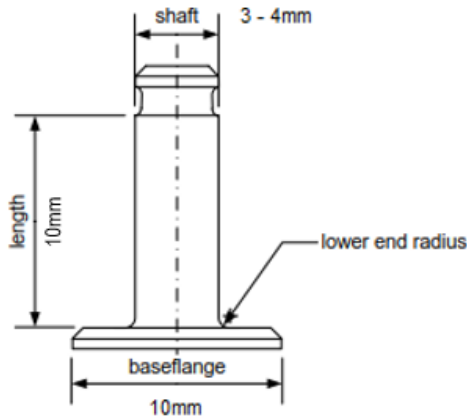


Figure 4-2: Generic dimensions of RUAG Standoffs, dependent of application and purpose

The MLI layer schematic provided by RUAG-A (Figure 4-3) shows the three different MLI blanket configurations that were tested.

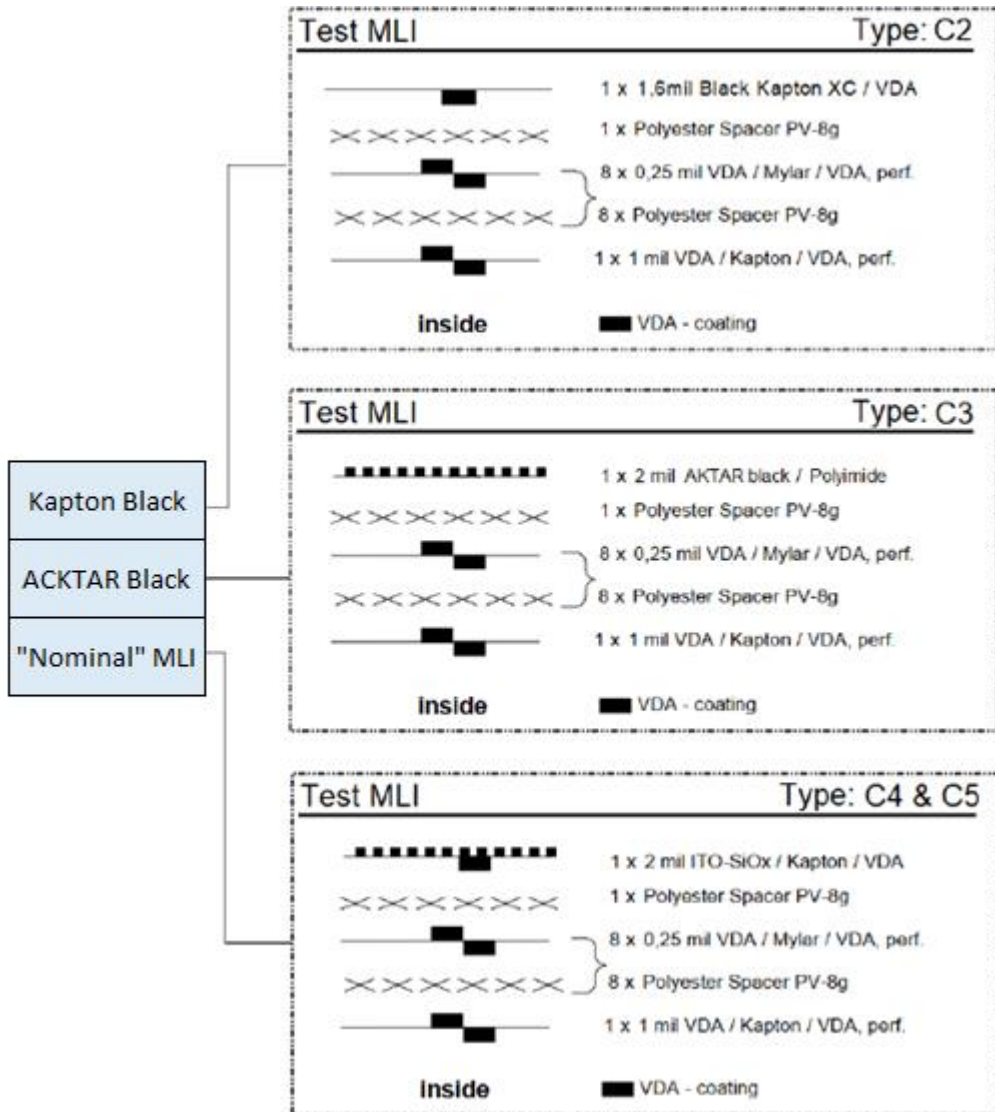


Figure 4-3: MLI layup configurations and their respective schematic diagrams

4.2 Velcro

Velcro is the second MLI connection method tested. It is used on particular satellites as a simple but effective method of MLI fixation to a spacecraft.



Figure 4-4: picture of ATOX MLI sample attached with Velcro

5 SAMPLE PREPARATION

The materials summarized in Table 5-1 are used for the D4D-BB specimen manufacturing. The used materials are based on common S/C structure configurations, for instance ExoMars TGO, Galileo, etc.

Table 5-1: Specimen Material Configuration

Application	Material Name	Remarks
ATOX Sample Material		
Faceskin	EX1515/M55J(6K)	0.6 mm thickness (8 plies)
Sandwich Material		
Faceskin	EX1515/M55J(6K)	Used for CFRP sandwich panel; 2 different lay-up types: <ul style="list-style-type: none"> 0.3 mm thickness (4 plies)
Honeycomb	PAMG-XR1-2.0-3/16-07-P-5056	19.4mm thickness
Insert Material		
Surface Insert	AA2024 - T851	
Through Spool Insert	AA2024 - T851	
Adhesives		
Adhesive Film	Redux 312UL	Used for Honeycomb/Faceskin Joint
Insert Potting Material	Stycast 1090/9	Used for Through Spool Inserts
Insert Potting Material	EY-3010 A/B	Used for Surface Inserts
Bracket Material		
Aluminium Cleat	AA7075 - T7351	

5.1.1 Test Substrate Design

The manufacturing of the substrates is performed according to flight hardware process definitions. This includes sandwich structure, autoclave cycle, curing conditions, (auxiliary) materials, NDT, dimensional checks etc. The specimens are manufactured with materials listed in Table 5-1.

The design of the panel substrates has been implemented as displayed in Figure 5-1 and Figure 5-2. The detailed specimen dimensions can be reviewed in the specimen drawings. The characterisation specimens are designed as single panel with standard dimensions of 80 mm by 80 mm with a through spool insert, see Figure 5-1 and Figure 5-2.

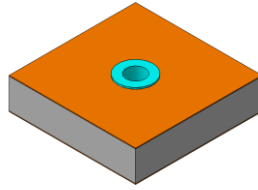


Figure 5-1: Characterisation specimen: 80 mm x 80 mm x 20 mm; Through Spool insert

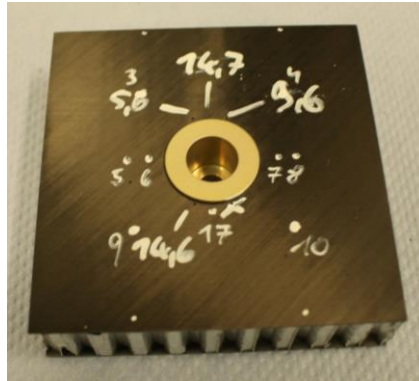


Figure 5-2: Manufactured CFRP sample with through spool insert

The corner sample test setup is designed with a setup of 2 panel specimen with dimensions of 160 mm by 160 mm. The specimen joints are based on state of the art flight hardware joint technologies and therefore connected by 2 edge inserts or by an additional bracket, as seen in Figure 5-3. This approach ensures that all three insert types can be tested in the phenomenology test campaign.

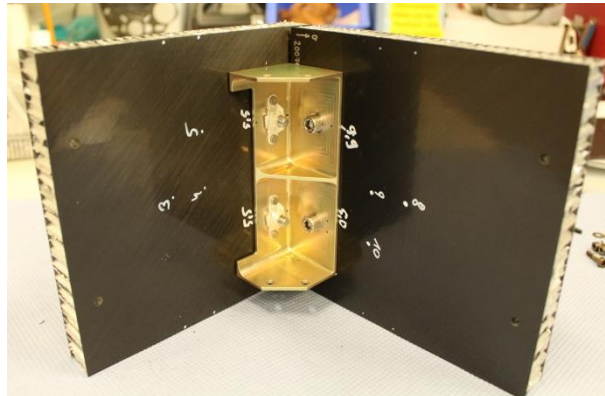
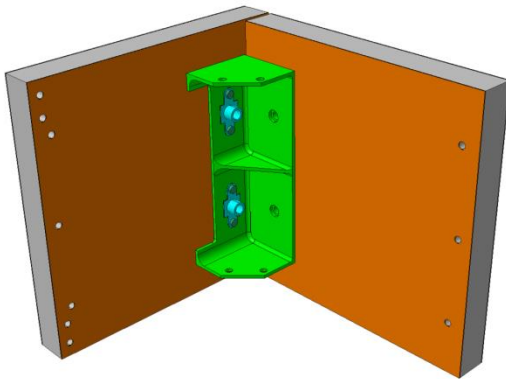


Figure 5-3 - Phenomenology specimen setup: 160 mm x 160 mm x 20 mm per panel; Cleat Joint via Through Spool and Surface Inserts (right: example of assembled CFRP panel setup)

6 ATOX TESTING

The atmospheric oxygen tests were performed at the ESTEC TEC-QEE LEOX facility, as shown in Figure 6-1.

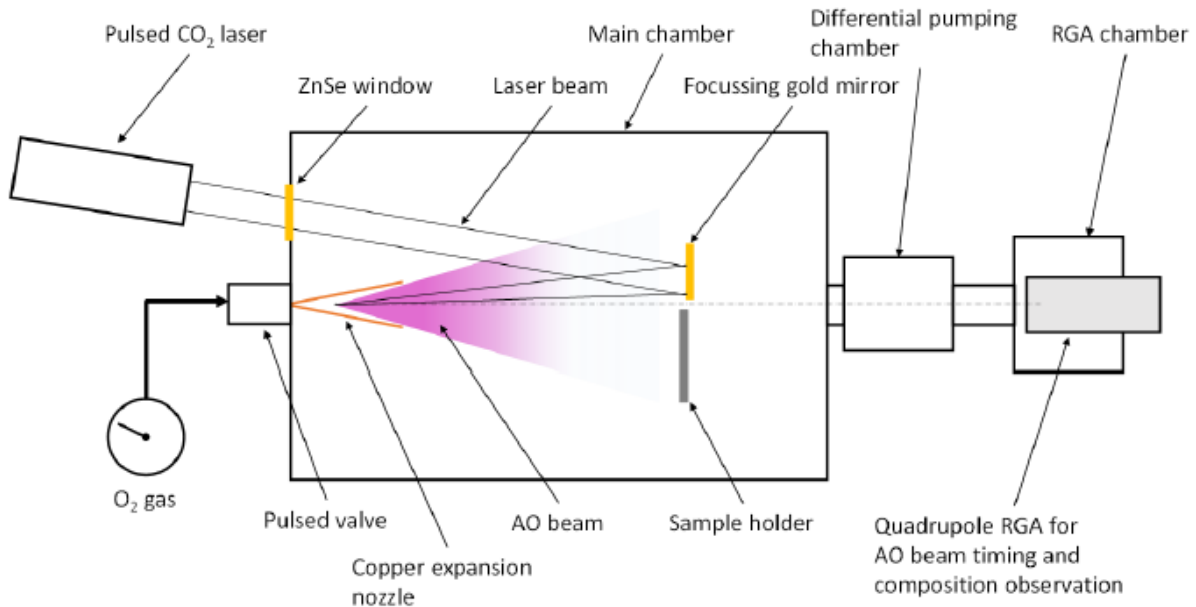


Figure 6-1: schematic of the ESTEC LEOX test facility

6.1 ATOX Test Samples

There was one smaller substrate design utilised for ATOX testing, and two for re-entry static testing. The ATOX test substrates can be seen highlighted in Figure 6-2.

The substrate used for the ATOX testing was a single face-sheet of CFRP. The single sheet was used to simulate the substrate surface of which the MLI and its respective connection technologies shall be adhered to, whilst also maintaining ease of connection to the respective test facility test apparatus.

The dimensions for the CFRP face-sheets was 114mm x 26mm, which also matched the MLI blanket dimensions being tested in the ATOX chamber.

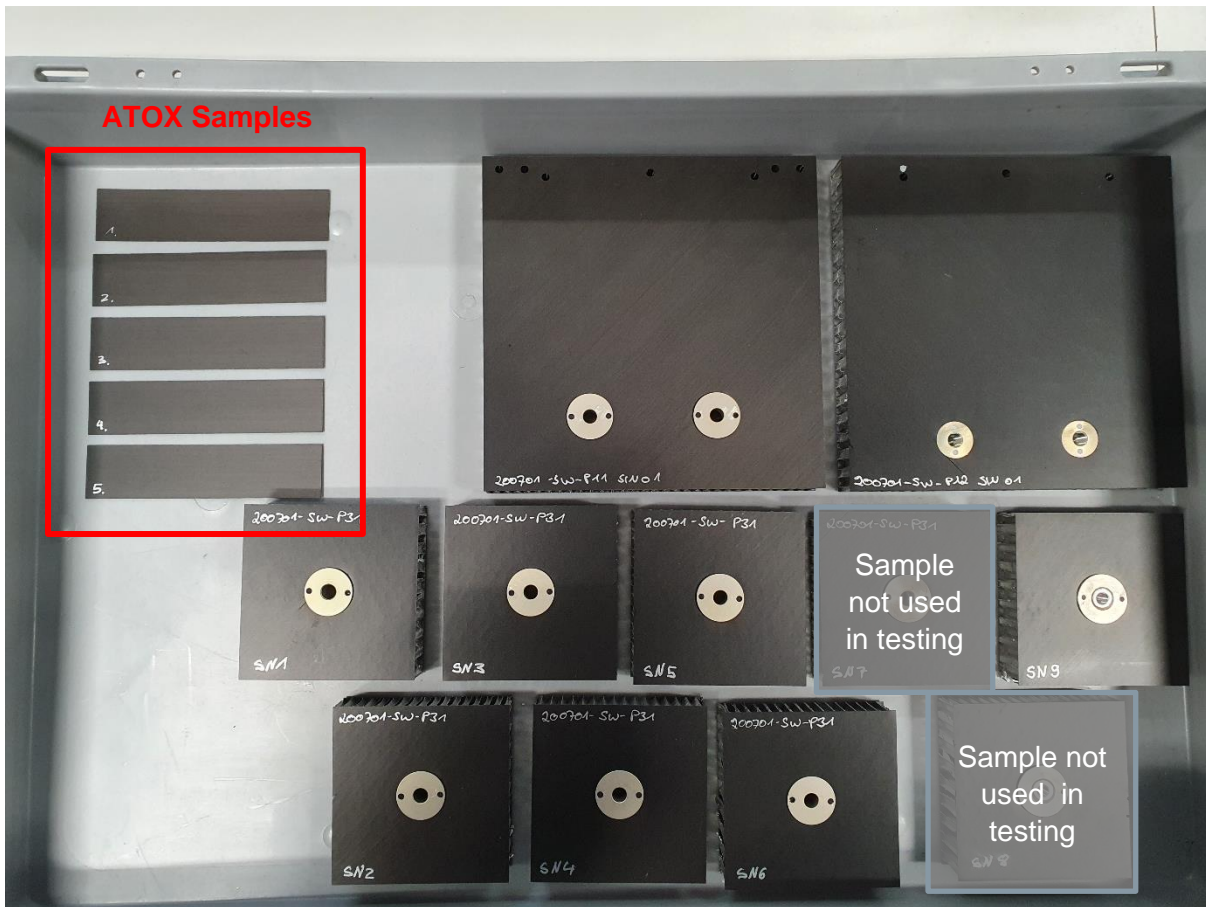


Figure 6-2: All samples as prepared from Invent

Table 6-1: as-manufactured ATOX sample information (courtesy of RUAG-A)

Config. Number	Test Type	MLI Configuration	Attachment Method	Size [mm x mm]	Mass [g]
1	Control	No MLI	-	26 x 114	2.8
2	Black Kapton XC/VDA	Black Kapton outer MLI layer	Velcro	26 x 114	5.8
3	ACKTAR black	Black paint applied to outer MLI layer	Velcro	26 x 114	6.1
4	“Nominal” MLI	ITO-SiOx outer MLI layer coating	Velcro	26 x 114	5.8
5	“Nominal” MLI	ITO-SiOx outer MLI layer coating	Stand-offs	26 x 114	7.1

6.2 Testing Results – ATOX Exposure

Atomic oxygen tests performed as an extension to the D4DBB study. It is based on an investigation of the atomic oxygen fluence on a spacecraft during de-orbit from a decaying circular orbit. The derivation of appropriate test conditions, and the assessment of the results are described. These tests provide information regarding the state of the spacecraft multi-layer insulation (MLI) at the start of the final re-entry process, as this is usually assumed to have been removed.

The results of the tests are clear; the impact of the atomic oxygen is minor on both a standard MLI surface and a CFRP surface.



Figure 6-3: pre-testing image of ATOX samples mounted to testing fixture

A desired test exposure of a fluence in the magnitude of approximately 3×10^{21} atoms/cm² was derived. However, as expected, there was a lower fluence applied to the samples during testing. These fluences are summarised in Table 6-2.

Table 6-2: fluence variation experienced on each sample

Sample	Location 1	Location 2	Location 3	Location 4	Average
Black Kapton	2.32e21	2.02e21	1.64e21	1.20e21	1.80e21
MLI (standoff)	2.63e21	2.34e21	1.91e21	1.43e21	2.08e21
CFRP	2.78e21	2.48e21	2.08e21	1.58e21	2.23e21
MLI (Velcro)	2.82e21	2.51e21	2.07e21	1.51e21	2.23e21
ACKTAR Black	2.66e21	2.34e21	1.88e21	1.36e21	2.06e21

There was a general symmetry of exposure expected as depicted in Figure 6-4. However, the exposure was centralised at a level found between the CFRP sample and the Velcro-equipped (ITO-SiOx) MLI sample below it.

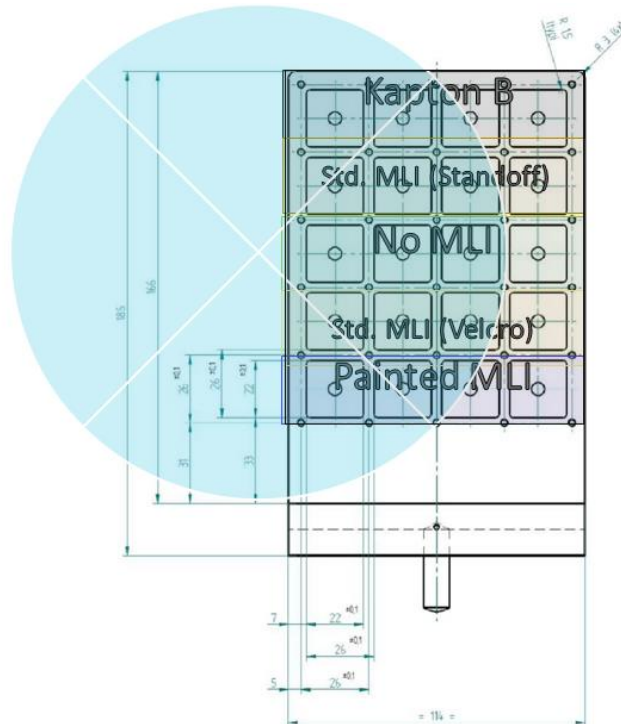


Figure 6-4: expectation of fluence applied across test samples

Once the ATOX test had concluded, there was a visual inspection, thermo-optical property measurement, SEM imaging, and a weight measurement performed.



Figure 6-5: post-testing image of ATOX samples mounted to testing fixture

The degradation of the Kapton loops on the standoff MLI sample can be clearly observed. However, no further erosion or degradation was visible to the eye on the remaining components of the sample.

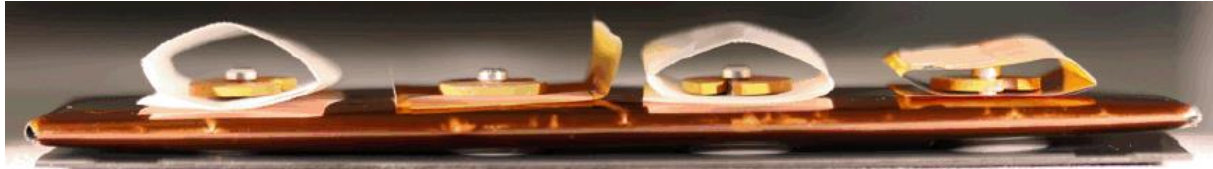


Figure 6-6: ITO-SiOx MLI sample utilising standoff mounting technologies post-ATOX exposure

The thermo-optical properties measured before and after testing did highlight some degradation experienced by the MLI samples. These properties are shown in Table 6-3.

Table 6-3: pre and post ATOX testing thermo-optical properties

Sample	Thermal Emittance		Solar Absorptance	
	Start	End	Start	End
Kapton Black	0.84	0.93	0.91	0.99
CFRP	0.81	0.85	0.89	0.98
Standard MLI (Velcro)	0.74	0.79	0.36	0.37
ACKTAR Black	0.84	0.85	0.97	0.97

The over-all mass-loss experienced by each sample was measured before test commencement, an interim inspection point (IIP) during the campaign, and after the conclusion of ATOX testing. These results are summarised in Table 6-4. A comparative evaluation of the erosion yields is found in Table 6-5.

Table 6-4: sample mass loss and corresponding atomic oxygen erosion yield experienced

Sample number	Mass measured at			Mass loss at		AO erosion yield till	
	BOT (g)	IIP (g)	EOT (g)	IIP (g)	EOT(g)	IIP (cm ³ /atom)	EOT (cm ³ /atom)
S1	5.81172	5.78664	5.6949	0.025	0.117	1.6 · 10 ⁻²⁴	1.5 · 10 ⁻²⁴
S2	7.08635	7.06589	7.0019	0.020	0.084	1.1 · 10 ⁻²⁴ (*)	9.1 · 10 ⁻²⁵ (*)
S3	2.77799	2.75997	2.7312	0.018	0.047	9.2 · 10 ⁻²⁵	4.7 · 10 ⁻²⁵
S4	5.81275	5.81215	5.7960	0.001	0.017	3.1 · 10 ⁻²⁶	1.7 · 10 ⁻²⁵
S5	6.11860	6.12154	6.1116	-0.003	0.007	-1.6 · 10 ⁻²⁵ (**)	7.6 · 10 ⁻²⁶

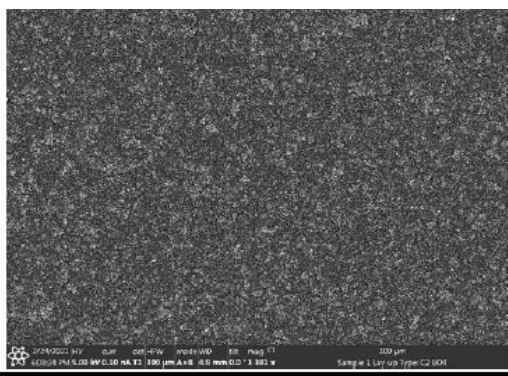
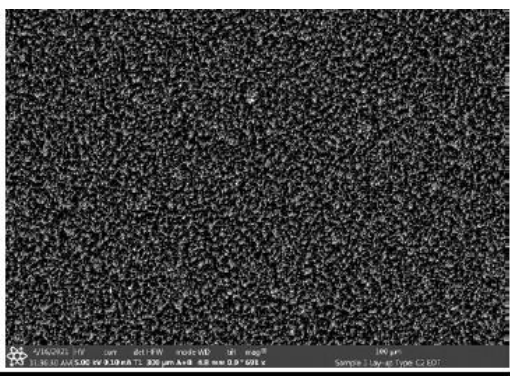
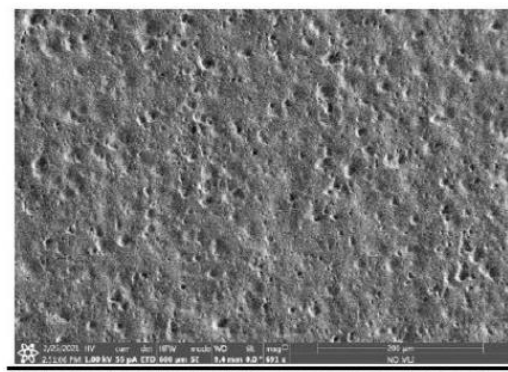
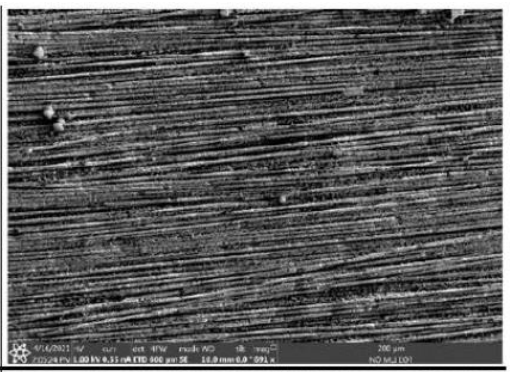
Note: in Table 6-4, S1 is Kapton black, S2 is ITO-SiOx with standoffs, S3 is CFRP, S3 is ITO-SiOx with Velcro, and S5 is ACKTAR black.

Table 6-5: relative erosion yield data

Sample No.	Material	Erosion Yield	Relative Erosion Yield
Ref.	Kapton (reference)	2.8e-24	1.0
1	Kapton Black	1.5e-24	0.5
2	Kapton protective loops	2.7e-24	1.0
3	CFRP	4.7e-25	0.2
4	Standard MLI	1.7e-25	0.06
5	Acktar Black	7.6e-26	0.03

The SEM imaging showed erosion behaviour that appeared to correlate to the numerical analyses and measurements taken during the ATOX test campaign. These images can be seen in Table 6-6.

Table 6-6: SEM imaging before and after ATOX exposure

Sample No.	Before Exposure	After Exposure
1		
2	Not analysed (same material and similar exposure to sample 4)	
3		

Sample No.	Before Exposure	After Exposure
4		
5		

As a point of interest, the ACKTAR Black sample was intentionally scratched in between the staples mounting the Velcro patches to the MLI sample. The SEM analysis regions can be seen in Figure 6-7.

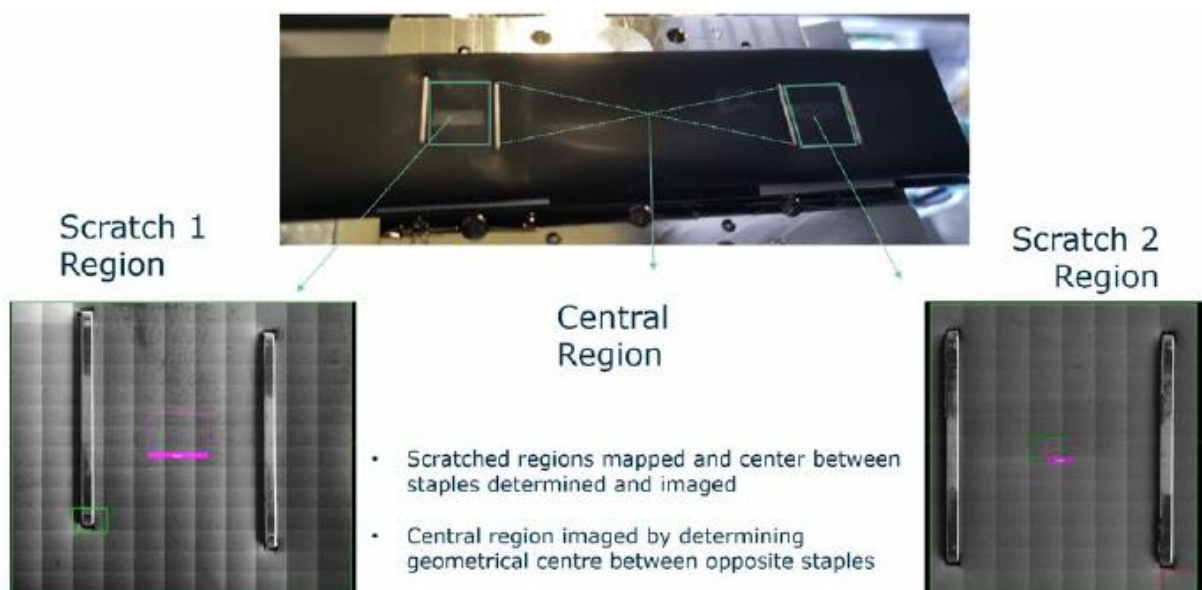


Figure 6-7: SEM measurement locations for ACKTAR black MLI sample

It was also visually noted that the Velcro was not degraded by ATOX exposure. This can be seen in Figure 6-8.

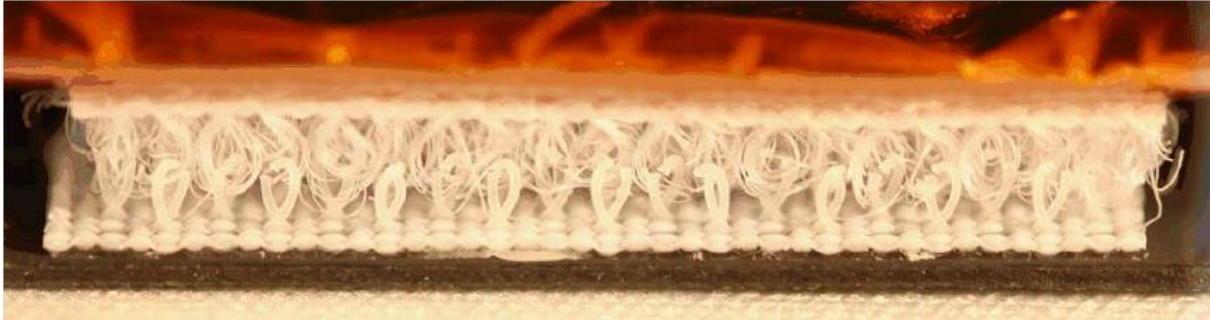


Figure 6-8: visual inspection of Velcro connection patches post-ATOX exposure

The ATOX exposure had no noticeable or critically detrimental effects on any of the MLI configurations tested under the predetermined exposure conditions. There were very few optical and physical changes in the appearance and function of the untested MLI blankets (Figure 6-9) themselves when compared to tested samples (Figure 6-10).



Figure 6-9: untested ITO-SiOx MLI blanket

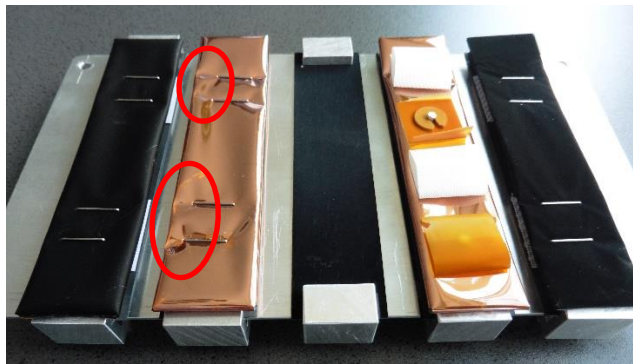


Figure 6-10: ATOX MLI samples post-testing with noticeable appearance change highlighted

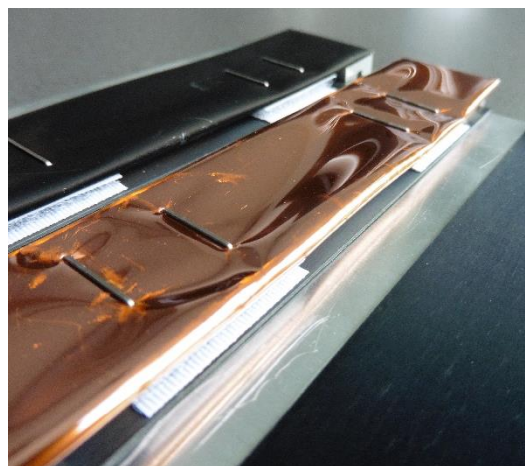


Figure 6-11: bright stripes observed on the outer layer of ITO-SiOx MLI

7 STATIC RE-ENTRY TESTING

Test Samples:

1 corner sample consisting of two 160mm x 160mm panels with different joining techniques, as well as seven 80mm x 80mm panels were tested. One of the 80mm x 80mm panels also tested a demisable insert manufactured employing a threaded insert that is soldered into place.

Test Setup:

A specially designed radiation heater for up to 100kW/m² had been manufactured and placed 20mm in front of the closest point of the sample. A purge gas flow was installed around the heater to prevent coating of the heater elements with the outgassing hydrocarbons.

Nominal heat flux:

The tests were run at typical heat flux profile (HF TRAJ) for the first stage of a spacecraft reentry into the atmosphere with a maximum of 50kW/m².

Mechanical Load:

The tests were performed with a static load of 20N per insert.

The mechanical load was applied at a previously determined angle as seen in Figure 7-1, right picture.

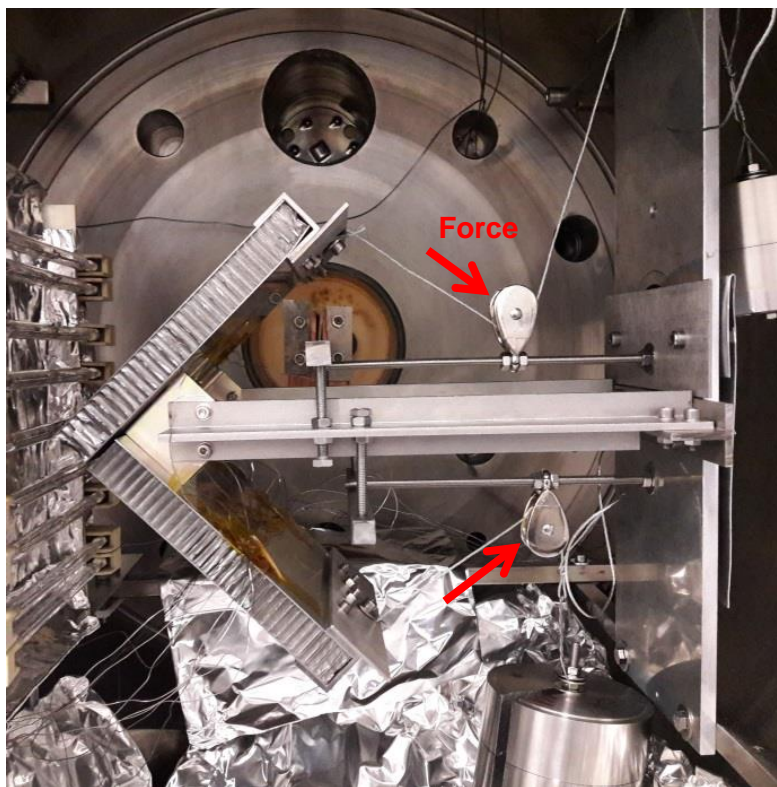


Figure 7-1: mechanical loading in chamber

7.1 Test Conditions Derivation

The derivation of appropriate test conditions for the D4DBB study was based on an investigation of the environmental loads on a spacecraft during the altitudes of interest during re-entry. The focus of the work has been on the 80-90km altitude range, with 85km taken as a nominal break-up altitude of interest.

The derivation of the environmental conditions of interest has been performed using the SAM tool, with support provided by the SCARAB simulations of the EnMap spacecraft, which is being used as the D4DBB study case. Good consistency has been seen in the conditions produced, providing a high level of confidence.

Analysis of the expected loading on the joints has also been performed, again using the SAM tool with support from the SCARAB EnMap simulations and from the OHB Finite Element model of EnMap, which is able to account for some of the effects of deformation which is not considered in the simplified models in the re-entry tools. This has shown that the deformation is important, but has resulted in magnitudes of the forces on the joints which are reasonably consistent with the more simple methods.

Some assessment has also been made of the heat soak through a sandwich panel using a 1D conduction model embedded within SAM. This has suggested that the gradual heat soak through the panel in the early stages of the re-entry can result in different temperature gradients that might be seen at a constant heat flux condition in a test facility. Thus, it is recommended that a re-entry trajectory condition with this long period of gradually increasing flux is used in the static facility to ensure that this phenomenology is covered. This is a change from the initial concept where constant fluxes representative of altitudes of interest were considered.

The low fluxes required for this re-entry condition are only achievable in the static re-entry chamber. Therefore, the static facility is used for the comparison of the trajectory effects with constant flux effects. The arc-heated wind tunnel is run at very low heat flux conditions in this activity, which are well outside the usual range of operation. This allows read-across at the constant flux condition from the static facility in order to provide some understanding of the flow effects.

The constant flux condition selected is 50kW/m², with an applied force of 20N per insert. The re-entry trajectory fluxes are based on SAM simulations used in the original breadboarding study, and the following profile was utilised.

Table 7-1: heat flux trajectory profile (HF TRAJ)

Time (s)	Heat Flux (kW/m ²)
0	3.2
285	3.2
465	5
765	20
965	50

7.2 Static Re-entry Substrate Design

The sample design for demisability testing is 80 x 80mm single panel, and two 160 x 160mm panels joined by a clevis. The individual sample specifications are outlined in Table 7-2. The load that shall be exerted on a select number of samples shall be a 20N static load. Although these loads may not be exactly in line with what is anticipated in flight, they are in line with previous test conditions.

7.2.1 Sample Mounting

Regarding the 80 x 80mm samples, the mounting solutions for use at AAC have been modified from the original design specifications so as to avoid significant negative impacts on the test outcomes. The as-designed sample holder can be seen in Figure 7-2, and the modified sample holder in Figure 7-3.

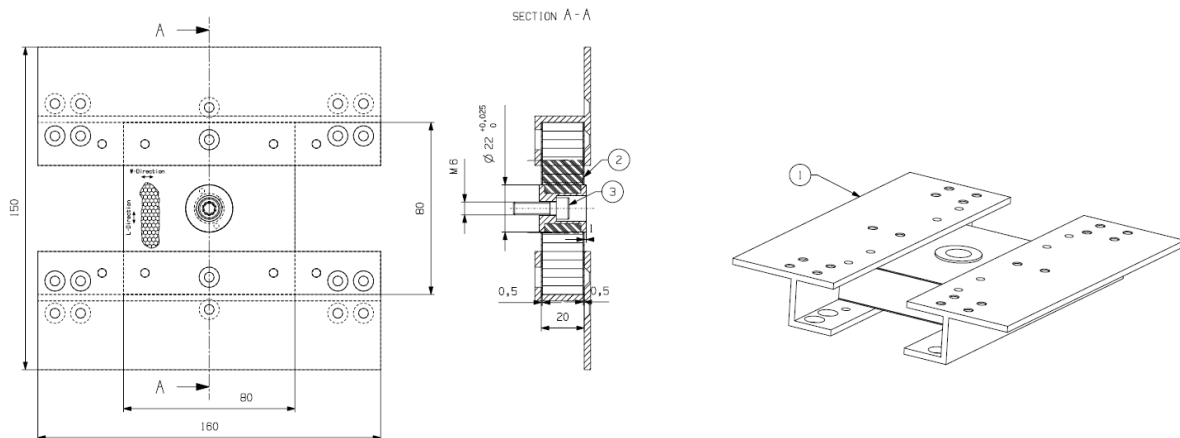


Figure 7-2: the 80 x 80mm sample holder as designed



Figure 7-3: picture with modified 80 x 80mm sample holder

The corner sample consisting of two 160mm x 160mm samples joined by a clevis were also attached to the test stand at the same clevis, as can be seen in Figure 7-1 and Figure 7-4.



Two-panel test samples and rigs



One-panel test samples and rigs

Figure 7-4: images showing use of sample mounting solutions (samples from previous D4D-BB testing)

7.3 Static Re-entry Testing

Static demise testing was performed in order to understand the effect of Multi-Layer Insulation (MLI) on the heating of a re-entering spacecraft. The test campaign and rebuilding performed here follows on from a previous campaign where it was determined that MLI will be essentially undamaged at the start of re-entry.

The presence of the MLI has been shown to have a clear effect on the heating of the underlying sandwich panel. The heating reduction is about 50% early in the trajectory, but this reduction increases as the heat flux increases. This is captured well by a 1D conduction model of the MLI, and has allowed the construction of a proxy model for the heat flux inhibition of the MLI which has been successfully prototyped within SAMj.

The removal of the MLI is highly dependent upon the connection method. MLI attached by Velcro is relatively easily removed, as the Velcro melts at about 150°C, resulting in the MLI detaching whilst the front facesheet remains intact. MLI attached by standoffs, however, is not removed easily. Indeed, the MLI begins to warp at about 200°C, resulting in more heat being able to reach the sandwich panel, but the standoffs do not fail, leaving the MLI in place. Eventually, at about 350°C, the adhesive connecting the front facesheet to the sandwich panel fails, and the MLI is removed from the panel, still attached to the front facesheet. This results

in a significant impact on the altitude at which the joints on a spacecraft would be expected to fail.

Previous studies showed a high altitude of joint failure, at about 95km. This was significantly higher than had been expected. Use of MLI with standoffs reduces this altitude to 82km, which is more in line with observations, although it should be noted that the observations are on steeper trajectories than the one simulated here. This adds confidence to the hypothesis that the MLI effect measured in this test campaign is applicable to re-entry studies.

Given that the predicted fragmentation altitude is significantly reduced by the presence of MLI, the importance of demisable joints to enhance spacecraft structural break-up is clear. To this end, the testing of the demisable two-part insert has shown that this behaves as expected, and is able to fail prior to the warping of the MLI attached by standoffs. This insert will clearly promote the separation of spacecraft panels, although there is a question as to whether this will be inhibited for some time by the presence of MLI in the case where the standoff attachment method is used.

The test matrix given in Table 7-2 shows the test samples, parameters, and sample-specific information.

Table 7-2: Sample specifications for re-entry demisability testing.

Test ID	Panel S/N	Test Condition	Applied Load	MLI Config. Type	Tech Config.	MLI Fixation	Insert Type	Panel Setup
1	SN6	TC2	20	N/A	No MLI	N/A	Spool	Control / 80x80
2	SN1	TC2	20	C5	Unaged MLI	Stand-offs	Spool	80x80
3	SN2	TC2	20	C4	Unaged MLI	Velcro	Spool	80x80
4	N/A (ATOX)	TC2	None	C5 w/ stand-offs	Exposed Sample 2 with MLI Coupon for same material	N/A	N/A	114 x 26 (ATOX)
5	SN5	TC2	20	C2	Unaged MLI	Stand-offs	Spool	80x80
6	SN4	TC2	20	C2	Unaged MLI	Velcro	Spool	80x80
7	N/A (ATOX)	TC2	None	C2 w/ velcro	Exposed Sample 4 with MLI Coupon for same material	N/A	N/A	114 x 26 (ATOX)
8	SN3	TC2	20	C3	Unaged MLI	Stand-offs	Spool	80x80
9	SN9	TC2	20	C5	Unaged MLI with Demisable Insert	Stand-offs	Demisable Spool	80x80
10	S/N01 (2 panels)	TC2	20	Unaged, C5	overlapping unaged MLI	Stand-offs	2 x Spool and 2 x Standard	2x 160x160

There was a noticeable difference in sample demise timescales when testing samples with MLI compared to the previous Breadboarding tests conducted (without MLI).

It was also noted that the standoffs remained intact throughout the duration of the tests, but the Velcro MLI connections demised at approximately 150°C.



Figure 7-5: corner sample (with standoffs) post-static re-entry testing

7.3.1 Test Calibration

To assist in consistency of results, the calibration data of the previous testing was used to calibrate the test facility for the CCN testing performed.

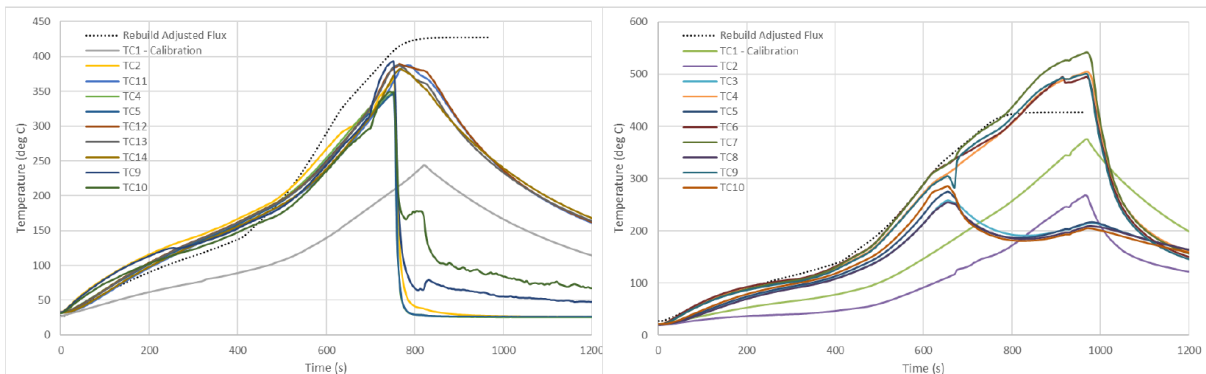


Figure 7-6: Calibration Blocks (CCN, left, and BB test campaign 2, right)

When comparing the calibration graphs in Figure 7-6, it can be seen that the CCN calibration data (left graph) shows higher initial heating, and lower heating later in the test. The data appears to show a lower peak temperature reached. The peak temperatures of both CCN and TC2 calibrations are in the same temperature range just before the 800 seconds mark.

However, after this, the CCN thermocouple 1, 2, 5, and 10 data drops off rapidly. This indicates a failure of the test specimen.

7.3.2 Static Re-entry Test Results

It can be seen in Figure 7-7 that the MLI provides an insulating effect, which results in approximately more than 20% increase in heating times to the same ~400°C peak temperatures measured in the Nominal MLI test when compared to the baseline test.

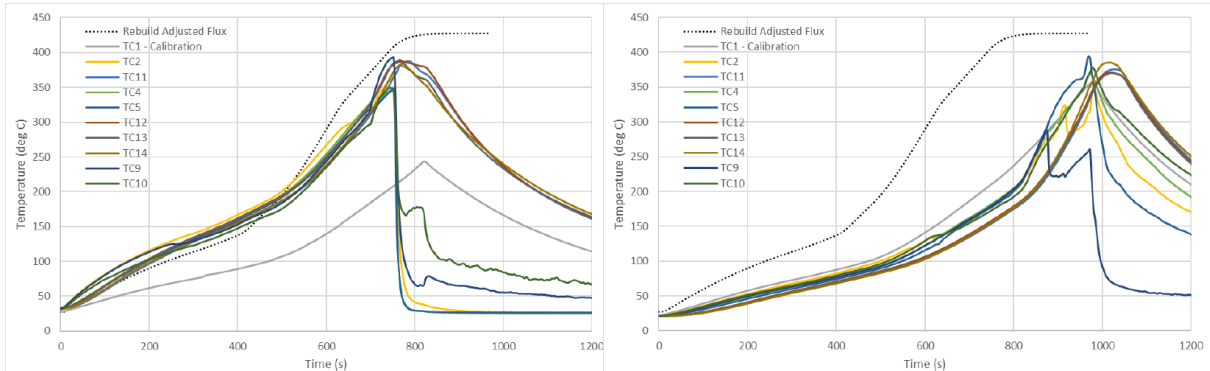


Figure 7-7: Baseline data, left, vs Nominal MLI, right)

The MLI installation technologies employed also dictated a noticeable change in demise characteristics of the over-all sample. The test sample experienced a much more gradual heating profile, whereas the Velcro-equipped sample experienced a noticeable heat rate increase above approximately 150°C. The described phenomena can be observed in Figure 7-8.

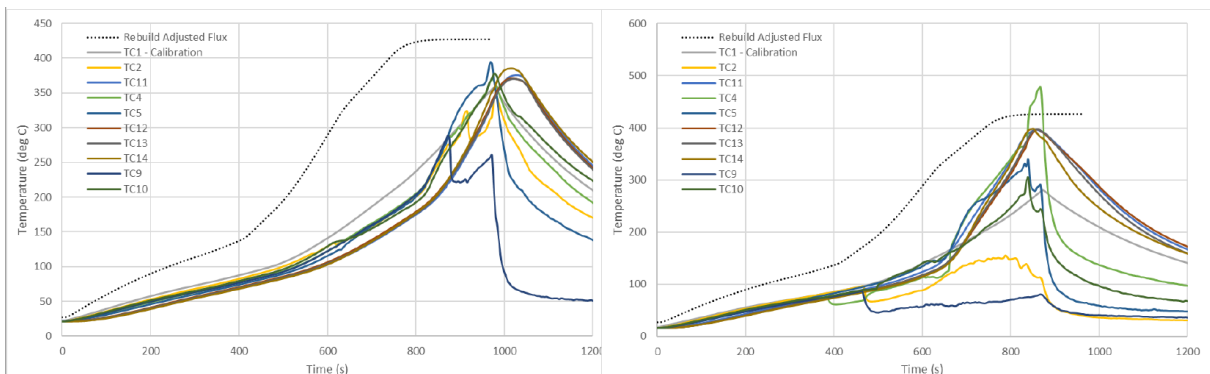


Figure 7-8: Nominal MLI (Standoffs, left, vs Velcro, right)

When comparing the nominal MLI vs Kapton black in Figure 7-9, it can be seen that the heating rate of Kapton black is slightly but noticeably higher. Most of the thermocouple peak temperatures of just under 400°C are also reached at approximately 950 seconds on the Kapton black sample, whereas the same approximate 400°C temperatures are reached at approximately 1050 seconds on the nominal MLI sample.

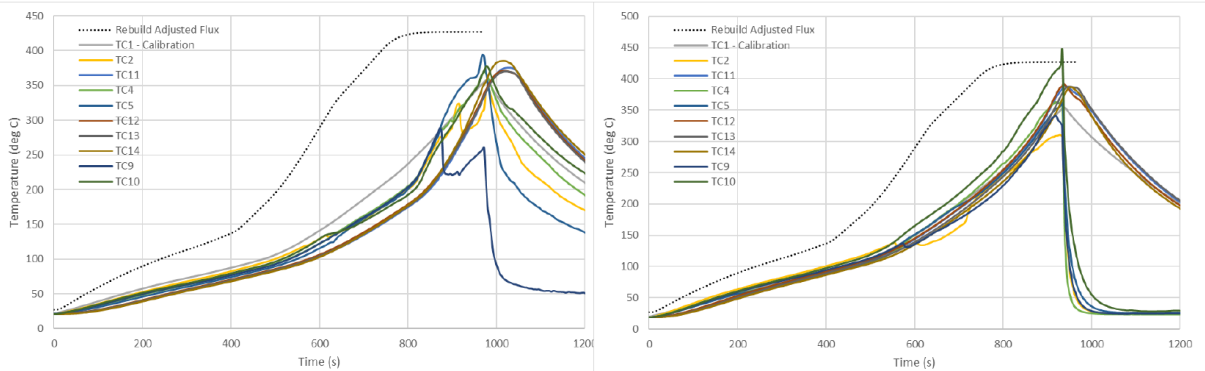


Figure 7-9: Nominal MLI vs Kapton Black (right), both utilising standoffs

When comparing the Velcro-equipped samples of both nominal MLI to the Kapton black (Figure 7-10), it can be noted that the same increased heating rate after 150°C is experienced on both samples. Both samples experience an approximately 400°C peak temperature on all thermocouples except for one on each respective sample. The Kapton Black sample (seen on the right of Figure 7-10) also saw these peak temperatures slightly earlier than the nominal MLI sample.

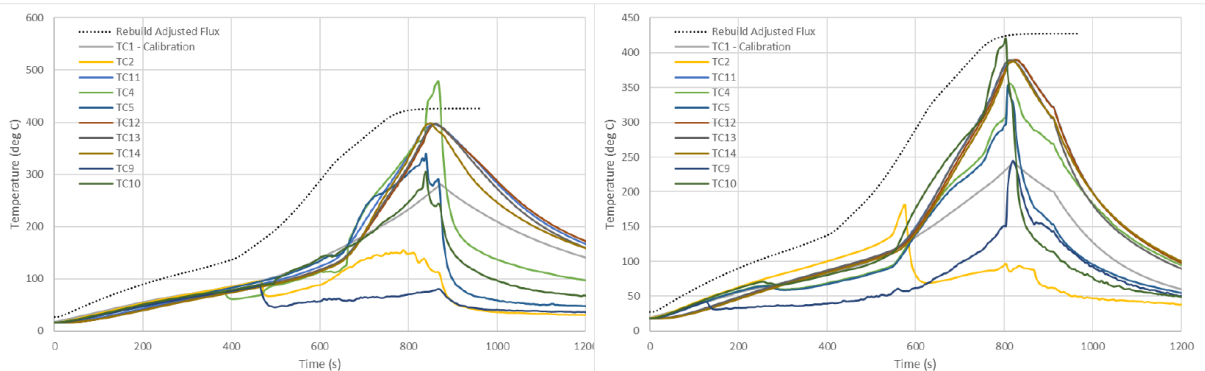


Figure 7-10: Nominal MLI vs Kapton Black (right) with Velcro

When comparing the test data from the baseline test to the ACKTAR black sample (Figure 7-11), it can be seen that there is a quite comparable heating profile between the ACKTAR black sample and the Kapton black samples. The experienced heating rate of the ACKTAR black sample is slightly faster than that of the baseline sample, and the maximum temperatures of the ACKTAR black sample also peaked slightly earlier.

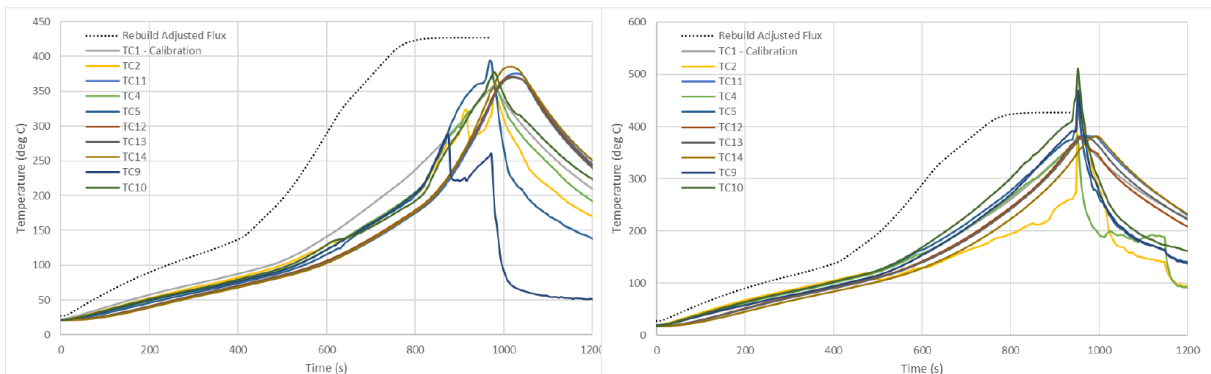


Figure 7-11: Baseline vs ACKTAR Black (right)

7.3.2.1 Demisable Insert Test

The bismuth-tin solder utilised in the demisable insert has a 140°C melting point. It was also noted that, with the total sample mass and the combined specific heat capacity of the bismuth-tin solder, a lower thermal inertia is achieved.



Figure 7-12: removal of bolt and threaded sleeve from the demisable insert body

When combining the lower thermal inertia of the sample with the added thermal insulation effects of the MLI blanket, and the slowed heating rate of the entire sample as seen in previous tests, a delay in demise of the insert was observed. In fact, once the relevant considerations were applied to the thermal model, it was noted that the effective melting point of the solder joint occurred once the surrounding temperatures reached 185°C (which is 725s after test commencement).

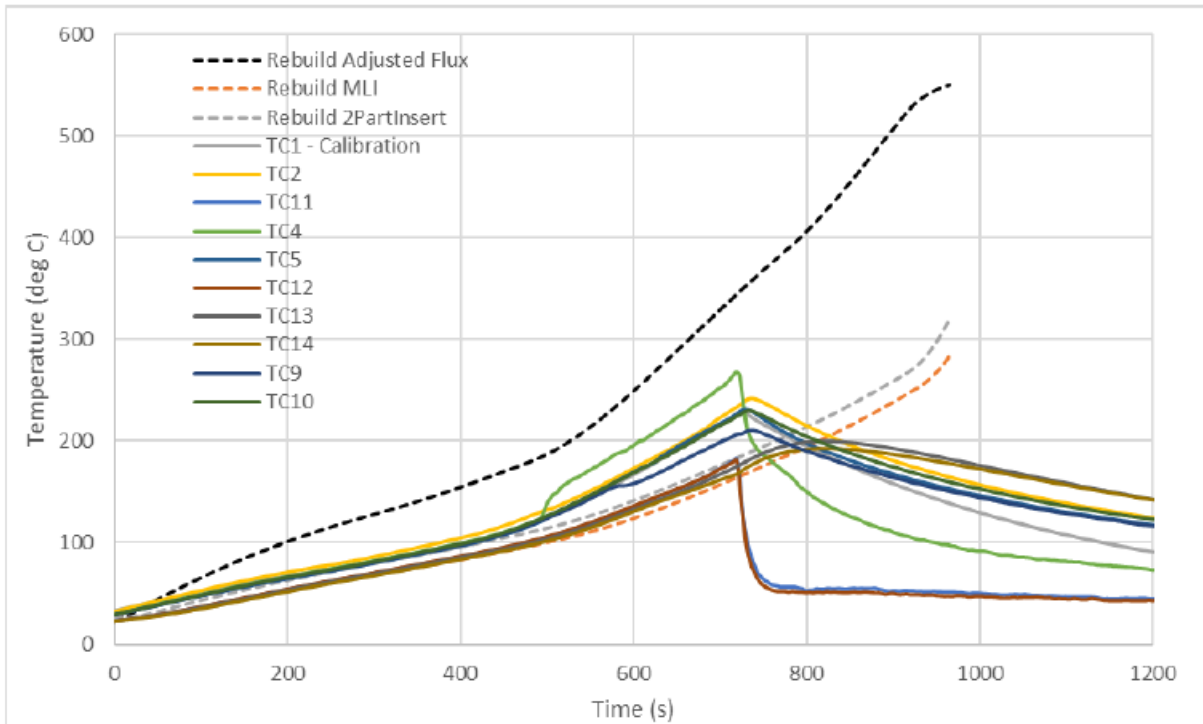


Figure 7-13: temperature measurements of demisable insert sample (Test ID 9)

7.3.2.2 Two-Panel Test

Testing of the two-panel 'corner sample' saw higher heat fluxes than what were observed in the smaller single-panel tests. However, the experienced heat fluxes in the locations of the inserts were lower by a factor of approximately two, and lowered significantly as the measurement points near the rear of the panels.



Figure 7-14: post-test damage of corner sample

The addition of MLI to the two-panel configuration provided a reduction in heat flux experienced by the panel. It must be noted that this observation is provided with a slightly conservative extrapolation of calibration data obtained in the 80mm x 80mm calibration. No specific calibration of the corner sample test was capable due to sample and test facility availability.

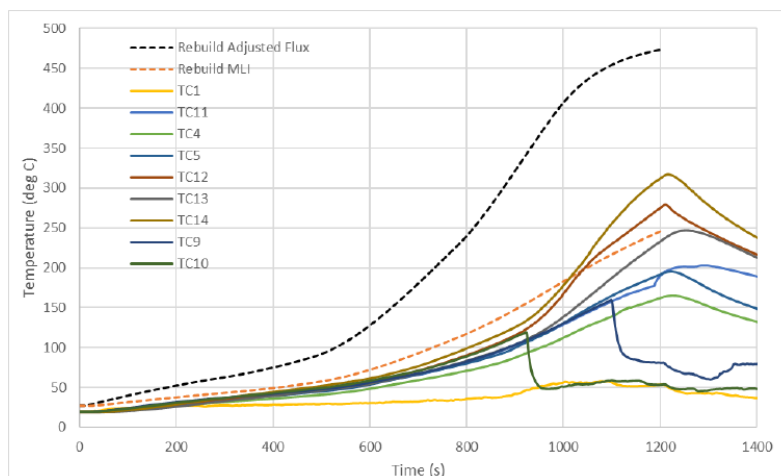


Figure 7-15: temperature data from corner sample test

As is highlighted in Figure 7-15, the MLI began to see demise after 20 minutes of testing. However, there was insignificant heat flux being imparted on the underlying substrate to induce

demise (and removal) of the facesheet. It was also noted that, as the MLI was attached to the sample with standoffs, the MLI remained attached to the test substrate throughout the duration of testing.

7.3.2.3 Atomic Oxygen Exposed Samples

Although these tests were performed as more a representative test to provide a basic level of comparison between virgin MLI and MLI that has seen simulated ATOX exposure.

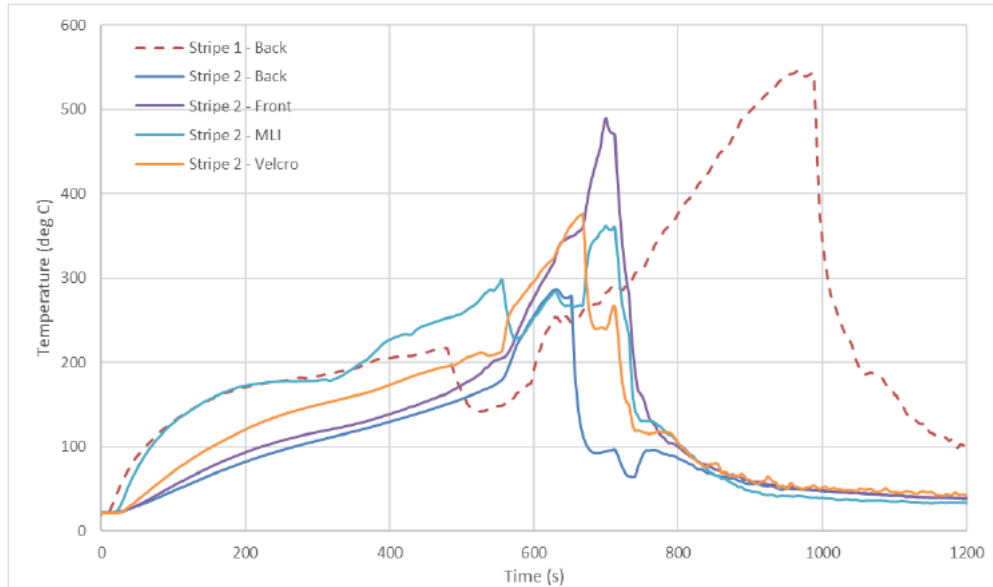


Figure 7-16: comparison of bare CFRP stripe and ATOX sample (Test ID 4) stripe

Although the thermocouple was attached with cho-foil, it can be seen in Figure 7-16 that the Stripe 1 test data experienced a partial detachment of the thermocouple from the substrate surface during testing.

The data also shows that the Velcro fails at approximately 200°C and the back face temperature is roughly 150°C (at 545 seconds into the test).

After analysis of the test data, a negligible effect on MLI demisability was seen due to previous ATOX exposure. However, the testing cannot be considered as quantitative due to the errors in data acquisition stemming from the connection of the sensors to the samples.

8 LESSONS LEARNED

To date, there have been some expectations coming from literature, and others coming from industry that have assumed particular demise characteristics of spacecraft componentry. Throughout the CCN activity, a reassessment of some of these assumptions has been required.

During ATOX testing, it was initially expected that the MLI would become slightly brittle, and that the Velcro patches used to connect the MLI to a substrate would degrade. However, this was not the case. The Velcro exhibited no visible degradation, and remained fully intact. This shows that Velcro degradation found in previous studies is likely due to other phenomena such as radiation. However, as there were no effects of solar radiation intentionally applied to the samples during testing, there were also no observable effects due to imparted (solar) radiation degradation observed. This could be interesting for future analysis.

The Kapton loops that protected the Vespel SP1 clip washers suffered severe degradation over the test campaign, with one of the loop's top halves completely detaching from the sample during testing. There was no visible degradation to any of the Vespel SP1 clip-washers. However, it was not possible to remove the clip-washers for more precise testing due to the test requirements of the required testing in the CCN.

The ACKTAR Black ATOX sample appeared to become slightly less glossy in appearance after testing completed. However, the appearance of this ATOX sample deviated the least visually from its pre-test condition. There was a scratch intentionally applied in the regions between the Velcro attachment staples of the ACKTAR Black sample (on both sides). These scratched regions exhibited no increase in degradation or demise due to ATOX exposure when compared to the rest of the sample. The ACKTAR Black sample also gained mass throughout the ATOX test, but recorded a net mass loss by the conclusion of the test. This mass fluctuation was theorised to be due to the formation of oxides on the MLI sample that were subsequently removed during the final phase of testing.

There was an interesting phenomena observed on the tested ITO-SiO_x ATOX samples where small, bright streaks in the MLI's outer layer appearance occurred. These streaks resemble stress-fracturing in ceramics. However, the topology of the ATOX MLI samples pre and post testing observed through SEM imaging did not indicate any notable mechanical failure. These bright streaks may have appeared in regions that were exhibited to notable localised stresses during installation and handling activities, but not enough is known on this to draw any conclusions of confidence.

When observing the Kapton Black sample, there was a notable difference in both the appearance of the Kapton black sample after ATOX testing had concluded. The sample was notably more matt in appearance, looking like more of a suede fabric than the smoother MLI sample it started as. The sample also experienced the most mass loss throughout testing.

The static re-entry testing conducted highlighted the critical nature of the presence of insulating materials such as MLI on a spacecraft exterior when experiencing re-entry.

It was seen that the presence of MLI increased the time required to heat the samples to the same temperatures by approximately 3 minutes. This time was reduced, however, with the use of Velcro as an MLI attachment method. It is believed that a combination of Velcro demise and failure of the Velcro patch adhesive enables the MLI blanket to detach from the underlying sample once a temperature of approximately 150°C is experienced through the re-entry heating profile employed during testing. Once the MLI blankets are able to release from the

samples; even partially, the underlying samples exhibit notable increases in rate of decomposition.

The thermo-optical properties of the respective MLIs tested had a not so insignificant role in the rate of demise in testing, however, these effects would not play a deciding role in the decomposition of a spacecraft.

9 CONCLUSION

The D4DBB CCN study has further solidified the understanding of demise greatly. The MLI materials currently used and how they react to re-entry conditions has been explored with significant gains in understanding and the potential evaluation of demise effects; having potential flow-on effects in how manufacturers design their spacecraft in the future. The limits of the previous understanding have been explored, gaining valuable knowledge of the representativeness of our analysis tools and highlighting a number of fronts in which assessments can be improved in the future. And whilst the limitations present in current testing capabilities cannot be ignored, the representativeness of the methodologies utilised have provided invaluable input into the modelling capabilities of demise due to spacecraft re-entry.

A selection of typical technologies were explored to different depths and the most promising of those in terms of future usage and knowledge to be gained were tested in a similar way to the current joining technologies in the D4DBB study previously. This has also expanded the understanding of the implementation and applicability of technologies for demise across satellites — as well as technologies that aid in demise prevention, and how this can be handled going into the future.